Inorg. Chem. **2002**, *41*, 6780–6789

New Oxamidato-Bridged Cu^{II}–Ni^{II} Complexes: Supramolecular Structures with Thiocyanate Ligands and Hydrogen Bonds. Magnetostructural Studies: DFT Calculations

Javier Tercero,[†] Carmen Diaz,*[,†] Joan Ribas,[†] Eliseo Ruiz,[†] José Mahía,[‡] and Miguel Maestro[‡]

Departament de Química Inorgànica, Universitat de Barcelona, Martí i Franquès, 1-11, 08028 Barcelona, Spain, and Servicios Xerais de Apoio a Investigación, Universidade da Coruña, Campus da Zapateira, s/n 15071, A Coruña, Spain

Received July 29, 2002

Four new supramolecular compounds of Cu^{II}–Ni^{II} have been synthesized and characterized: $[Cu(Me_2oxpn)Ni(\mu\text{-}NCS)(H_2O)(tmen)]_2(ClO_4)_2$ (**1**), $[Cu(Me_2oxpn)Ni(\mu\text{-}NCS)(H_2O)(tmen)]_2(PF_6)_2$ (**2**), $[Cu(oxpn)Ni(\mu\text{-}NCS)(NCS)\ (tmen)]_n$ (**3**), and $[Cu(Me_2oxpn)Ni(\mu\text{-}NCS)(NCS)(tmen)]_n$ (**4**), where oxpn = *N*,*N*′-bis(3-aminopropyl)oxamidate, Me_2oxpn = *N*,*N*′-bis(3-amino-2,2′-dimethylpropyl)oxamidate, and tmen = *N*,*N*,*N*′,*N*′-tetramethylethylenediamine. Their crystal structures were solved. Complexes **1** and **2** have the same tetranuclear cationic part but a different counteranion. The cationic part consists of two $[Cu(Me_2oxpn)Ni]$ moieties linked by SCN^- bridged ligands and intra-tetranuclear hydrogen bonds. In the case of complex **3**, a two-dimensional system was built, the thiocyanate ligand linking the dinuclear units gives a chain, and the chains are linked together by hydrogen bonds; intrachain hydrogen bonds are also present. For complex **4**, the thiocyanate ligands produce intermolecular linkages between the dinuclear entities, giving a one-dimensional system; intrachain hydrogen bonds are also present. The magnetic properties of the four complexes were studied by susceptibility measurements vs temperature. DFT calculations were made to study the contribution of the SCN^- and hydrogen bond bridges in the magnetic coupling.

Introduction

Molecules that contain two kinds of metal ions play an important role in molecular magnetism.[1,2] The magnetic interaction between two nonequivalent paramagnetic centers may lead to situations which cannot be encountered with species containing only one kind of center. One of the best strategies to design and synthesize heteronuclear species is the "complex as ligand" approach: using mononuclear complexes that contain potential donor groups for another metal ion.[3] A good example of this pathway is represented by the mononuclear Cu^{II} complexes of oxamidates[4] and oxamates.[5,6] Some coordination supramolecular arrays based on covalent interactions and/or hydrogen bonds in complexes with substituted oxamate[7−12] and oxamidate[13−17] complexes have been reported. Focusing on dinuclear Cu^{II}−Ni^{II} with

* Author to whom correspondence should be addressed. E-mail: carme.diaz@qi.ub.es.
† Universitat de Barcelona.
‡ Universidade da Coruña.

(1) Kahn, O. *Adv. Inorg. Chem.* **1996**, *43*, 179.
(2) Kahn, O. *Struct. Bonding (Berlin)* **1987**, *68*, 89.
(3) Aukauloo, A.; Ottenwaelder, X.; Ruiz, R.; Journaux, Y.; Pei, Y.; Rivière, E.; Muñoz, C. *Eur. J. Inorg. Chem.* **2000**, 951 and references therein.
(4) Ruiz, R.; Faus, J.; Lloret, F.; Julve, M.; Journaux, Y. *Coord. Chem. Rev.* **1999**, *193*−*195*, 1069.
(5) Stumpf, H. O.; Pei, Y.; Kahn, O.; Sletten, J.; Renard, J. P. *J. Am. Chem. Soc.* **1993**, *115*, 6738.
(6) Gao, E. Q.; Tang, J. K.; Liao, D. Z., Jiang, Z. H.; Yan, S. P.; Wang, G. L. *Inorg. Chem.* **2001**, *40*, 3134.
(7) Tercero, J.; Diaz, C.; El Fallah, M. S.; Ribas, J.; Maestro, M. A.; Mahía, J. *Inorg. Chem.* **2001**, *40*, 3077.
(8) Tercero, J.; Diaz, C.; Ribas, J.; Mahía, J.; Maestro, M. A.; Solans, X. *J. Chem. Soc., Dalton Trans.* **2002**, 2040.
(9) Gao, E. Q.; Zhao, Q. H.; Tang, J. K., Liao, D. Z.; Jiang, Z. H.; Yan, S. P.*J. Chem Soc., Dalton Trans.* **2001**, 1537.
(10) Ribas, J.; Diaz, C.; Solans, X.; Font-Bardía, M. *Inorg. Chim. Acta* **1995**, 229.
(11) Ribas, J.; Diaz, C.; Solans, X.; Font-Bardía, M. *J. Chem. Soc., Dalton Trans.* **1996**, 35.
(12) Unamuno, I.; Gutierrez-Zorrilla, J. M.; Luque, A.; Román, P.; Lezama, L.; Calvo, R.; Rojo, T. *Inorg. Chem.* **1998**, *37*, 6452.
(13) Lloret, F.; Julve, M.; Faus, J.; Journaux, Y.; Philoche-Levisalles, M.; Jeannin, Y. *Inorg. Chem.* **1989**, *28*, 3702.
(14) Zhang, H. X.; Kang, B. S.; Zhou, Z. Y.; Chan, A. S. C.; Chen, Z. N.; Ren, C. *J. Chem Soc., Dalton Trans.* **2001**, 1664.
(15) Zhang, H. X.; Kang, B. S.; Xu, A. W.; Chen, Z. N.; Zhou, Z. Y.; Chan, A. S. C.; Yu, K. B.; Ren, C. *J. Chem Soc., Dalton Trans.* **2001**, 2559.
(16) Lloret, F.; Julve, M.; Real, J. A.; Faus, J.; Ruiz, R.; Mollar, M.; Castro, I.; Bois, C. *Inorg. Chem.* **1992**, *31*, 2956.

10.1021/ic025910r CCC: $22.00
Published on Web 11/15/2002

N,*N*′-bis(coordinating group substituted)oxamides, we found in the literature few complexes with a supramolecular array: tetranuclear systems in which the heterodinuclear entities are linked by thiocyanate ligand,[18] one-dimensional complexes in which the heterodinuclear entities are linked by nitrite group,[19] and a supramolecular structure in which the $Cu^{II}-Ni^{II}$ entities are linked by hydrogen bonds and behave as a molecular based magnet.[20] The magnetic coupling through the oxamidate(2−) ligand is well-known: the coupling is strongly antiferromagnetic, owing to the broad overlap between the magnetic orbital of the copper(II) and nickel(II) ions and the corresponding molecular orbital of the oxamidate ligand.[21] In molecular magnetism, not only local spins associated with metal ions but also the molecular spins associated with molecular units as a whole are important. Thus, we focused our interest on the association of the "molecular spins" (dinuclear entities) that takes place when the supramolecular assemblies are formed.

With these facts in mind, four new compounds, $[Cu(Me_2oxpn)Ni(\mu\text{-}NCS)(H_2O)(tmen)]_2(ClO_4)_2$ (**1**), $[Cu(Me_2oxpn)Ni(\mu\text{-}NCS)(H_2O)(tmen)]_2(PF_6)_2$ (**2**), $[Cu(oxpn)Ni(\mu\text{-}NCS)(NCS)(tmen)]_n$ (**3**), and $[Cu(Me_2oxpn)Ni(\mu\text{-}NCS)(NCS)(tmen)]_n$ (**4**), were prepared and characterized. The crystal structure and magnetic properties were investigated. DFT calculations were also made to study the contribution of the SCN^- and hydrogen bond bridges in the magnetic coupling.

Experimental Section

Materials. Nickel(II) perchlorate, nickel(II) nitrate, ammonium thiocyanate, ammonium hexafluorophospate, *N*,*N*,*N*′,*N*′-tetramethylethylenediamine (tmen), and acetonitrile were purchased from Aldrich and used without purification. The [Cu(oxpn)] and [Cu(Me$_2$oxpn)] compounds, where oxpn and Me$_2$oxpn are the dianions of *N*,*N*′-bis(3-aminopropyl)oxamide and *N*,*N*′-bis(3-amino-2,2′-dimethylpropyl)oxamide, respectively, were synthesized as previously described.[22,23] Ethanol was distilled before being used.

CAUTION! Although no problems were encountered in this work, perchlorate salts containing organic ligands are potentially explosive. They should be prepared in small quantities and handled with care.

Syntheses. $[Cu(Me_2oxpn)Ni(\mu\text{-}NCS)(H_2O)(tmen)]_2(ClO_4)_2$ (1). An ethanolic solution (60 mL) of $Ni(ClO_4)_2\cdot 6H_2O$ (0.5 g, 1.36 mmol) was added to a stirred solution of *N*,*N*,*N*′,*N*′-tetramethylethylenediamine (tmen) (0.159 g, 1.36 mmol) in ethanol (20 mL). Solutions of [Cu(Me$_2$oxpn)] (0.435 g, 1.36 mmol) in water (30 mL) and NH_4SCN (0.104 g, 1.36 mmol) in ethanol (20 mL) were then added consecutively. The resulting blue solution was filtered to remove any impurity and left to evaporate slowly at room temperature. Violet monocrystals suitable for X-ray determinations were collected after 2 weeks (yields ca. 60%). Anal. Calcd for $C_{19}H_{42}ClCuN_7NiO_7S$: C, 34.04; H, 6.32; N, 14.62; Cl, 5.29; S, 4.78. Found: C, 34.2; H, 6.3; N, 14.6; Cl, 5.2; S, 4.7.

$[Cu(Me_2oxpn)Ni(\mu\text{-}NCS)(H_2O)(tmen)]_2(PF_6)_2$ (2). This compound was prepared like complex **1**, using $Ni(NO_3)\cdot 6H_2O$ instead of $Ni(ClO_4)_2\cdot 6H_2O$. Finally, a solution of NH_4PF_6 (0.222 g, 1.36 mmol) in ethanol (20 mL) was added. Violet monocrystals suitable for X-ray determinations were collected after 1 week (yield ca. 65%). Anal. Calcd for $C_{19}H_{42}CuF_6N_7NiO_3PS$: C, 31.88; H, 5.91; N, 13.69; S, 4.47. Found: C, 32.2; H, 5.9; N, 13.6; S, 4.4.

$[Cu(oxpn)Ni(\mu\text{-}NCS)(NCS)(tmen)]_n$ (3). A solution of $Ni(NO_3)_2\cdot 6H_2O$ (0.794 g, 2.73 mmol) in acetonitrile (30 mL) was added to a stirred solution of tmen (0.318 g, 2.73 mmol) in acetonitrile (15 mL). Solutions of [Cu(oxpn)] (0.72 g, 2.73 mmol) in water (30 mL) and NH_4SCN (0.304 g, 4 mmol) in acetonitrile (30 mL) were then added consecutively. The resulting blue solution was filtered to remove any impurity and left to evaporate slowly at room temperature. Violet monocrystals suitable for X-ray determinations were collected after 3 weeks (yields ca. 60%). Anal. Calcd for $C_{16}H_{32}CuN_8NiO_2S_2$: C, 34.63; H, 5.81; N, 20.20; S, 11.56. Found: C, 34.3; H, 5.9; N, 20.0; S, 11.4.

$[Cu(Me_2oxpn)Ni(\mu\text{-}NCS)(NCS)(tmen)]_n$ (4). A solution of $Ni(NO_3)_2\cdot 6H_2O$ (0.397 g, 1.36 mmol) in methanol (30 mL) was added to a stirred solution of tmen (0.159 g, 1.36 mmol) in methanol (20 mL). Solutions of [Cu(Me$_2$oxpn)] (0.435 g, 1.36 mmol) in ethanol (30 mL) and NH_4SCN (0.15 g, 2 mmol) in water (20 mL) were then added consecutively. The resulting blue solution was filtered to remove any impurity and left to evaporate slowly at room temperature. Violet monocrystals suitable for X-ray determinations were collected after 3 weeks (yields ca. 65%). Anal. Calcd for $C_{20}H_{40}CuN_8NiO_2S_2$: C, 39.32; H, 6.60; N, 18.34; S, 10.50. Found: C, 39.1; H, 6.7; N, 18.2; S, 10.3.

Crystal Data Collection and Refinement. Suitable crystals of **1** (block, violet, dimensions 0.30 × 0.25 × 0.10 mm), **2** (prism, violet, dimensions 0.35 × 0.30 × 0.25 mm), **3** (block, violet, dimensions 0.40 × 0.20 × 0.15 mm), and **4** (block, violet, dimensions 0.45 × 0.25 × 0.20 mm), were used for the structure determination. X-ray data were collected using a Bruker SMART CCD area detector single-crystal diffractometer with graphite-monochromatized Mo Kα radiation (λ = 0.71073 Å) by the $\phi-\omega$ scan method at room temperature. A total of 1271 frames of intensity data were collected for each compound. The integration process yielded a total of 10267 reflections for **1**, 18221 for **2**, 15811 for **3**, and 20011 for **4**, of which 7064 [R(int) = 0.0243], 7738 [R(int) = 0.0275], 5843 [R(int) = 0.0476], and 7048 [R(int) = 0.0250], respectively, were independent. Absorption corrections were applied using the SADABS[24] program (maximum and minimum transmission coefficients, 0.863 and 0.658 for **1**; 0.713 and 0.631 for **2**; 0.764 and 0.518 for **3**; and 0.743 and 0.537 for **4**). The structures were solved using the Bruker SHELXTL-PC[25] software by direct methods and refined by full-matrix least-squares methods on F^2. Hydrogen atoms were included in calculated positions and refined in the riding mode, less those of water molecules that were located on residual density maps, but then also refined in the riding mode. For **1**, convergence was reached at a final R1 = 0.0523 [for $I > 2\sigma(I)$], wR2 = 0.1421 [for all data], 342 parameters, with allowance for the thermal anisotropy for all non-hydrogen atoms. The weighting scheme employed was $w =$

(17) Chen, Z. N.; Qiu, J.; Wu, Z. K.; Fu, D. G.; Yu, K. B. *J. Chem. Soc., Dalton Trans.* **1994**, 1923.
(18) Ribas, J.; Diaz, C.; Costa, R.; Tercero, J.; Solans, X.; Font-Bardía, M.; Stoeckli-Evans, H. *Inorg. Chem.* **1998**, *37*, 233.
(19) Diaz, C.; Ribas, J.; Costa, R.; Tercero, J.; El Fallah, M. S.; Solans, X.; Font-Bardía, M. *Eur. J. Inorg. Chem.* **2000**, 675.
(20) Tercero, J.; Diaz, C.; Ribas, J.; Mahía, J.; Maestro, M. A. *Chem. Commun.* **2002**, 364.
(21) Escuer, A.; Vicente, R.; Ribas, J.; Costa, R.; Solans, X. *Inorg. Chem.* **1992**, *31*, 2627 and references therein.
(22) Ojima, H.; Nonoyama, K. *Z. Anorg. Allg. Chem.* **1972**, *398*, 75.
(23) Ribas, J.; Garcia, A.; Monfort, M. *Polyhedron* **1991**, *10*, 103.
(24) Sheldrick, G. M. *SADABS*; University of Göttingen: Göttingen, Germany, 1996. Program for absorption corrections using Bruker CCD data.
(25) Sheldrick, G. M. *Bruker SHELXTL-PC*; University of Göttingen: Göttingen, Germany, 1997.

Table 1. Crystallographic Data for **1**−**4**

	1	**2**	**3**	**4**
empirical formula	$C_{19}H_{42}ClCuN_7NiO_7S$	$C_{19}H_{42}CuF_6N_7NiO_3PS$	$C_{16}H_{32}CuN_8NiO_2S_2$	$C_{20}H_{40}CuN_8NiO_2S_2$
fw	670.36	715.88	554.87	610.97
space group	$P\bar{1}$	$P\bar{1}$	$P2(1)/c$	$P2(1)/c$
cryst syst	triclinic	triclinic	monoclinic	monoclinic
Z	2	2	4	4
a, Å	9.270(1)	9.639(1)	16.410(1)	14.119(2)
b, Å	12.839(1)	12.816(1)	8.425(1)	15.015(2)
c, Å	14.330(1)	14.445(1)	18.503(1)	13.519(2)
α, deg	109.439(1)	107.830(1)	90	90
β, deg	106.010(1)	108.381(1)	111.822(1)	91.883(2)
γ, deg	93.990(1)	93.915(1)	90	90
V, Å^3	1521.3(1)	1585.0(1)	2375.0(1)	2864.6(5)
ρ(calc), g/cm^3	1.463	1.500	1.552	1.417
μ_{calc}, mm^{-1}	1.521	1.449	1.893	1.577
radiation (Mo Kα), Å	0.70173	0.70173	0.70173	0.70173
T, K	298(2)	298(2)	298(2)	298(2)
θ range for data collection	1.6−28.0	1.6−28.3	1.3−28.3	2.0−28.3
final R indices[a]	R1 = 0.0523	R1 = 0.0415	R1 = 0.0527	R1 = 0.0364
[$I > 2\sigma(I)$]	wR2 = 0.1199	wR2 = 0.1009	wR2 = 0.1187	wR2 = 0.0874
final R indices	R1 = 0.0861	R1 = 0.0658	R1 = 0.1041	R1 = 0.0524
[for all data]	wR2 = 0.1421	wR2 = 0.1132	wR2 = 0.1489	wR2 = 0.0956

[a] $R1 = \sum||F_o| - |F_c||/\sum|F_o|$ and $wR2 = \{\sum[w(F_o^2 - F_c^2)^2]/\sum[w(F_o^2)^2]\}^{1/2}$.

$[\sigma^2(F_o^2 + (0.0614P)^2 + 1.5594P]$ and $P = (|F_o|^2 + 2|F_c|^2)/3$, and the goodness of fit on F^2 was 1.012 for all observed reflections. For **2** convergence was reached at a final R1 = 0.0415 [for $I > 2\sigma(I)$], wR2 = 0.1132 [for all data], 360 parameters, with allowance for the thermal anisotropy for all non-hydrogen atoms. The weighting scheme employed was $w = [\sigma^2(F_o^2 + (0.0498P)^2 + 0.8199P]$ and $P = (|F_o|^2 + 2|F_c|^2)/3$, and the goodness of fit on F^2 was 1.028 for all observed reflections. For **3** convergence was reached at a final R1 = 0.0527 [for $I > 2\sigma(I)$], wR2 = 0.1489 [for all data], 275 parameters, with allowance for the thermal anisotropy for all non-hydrogen atoms. The weighting scheme employed was $w = [\sigma^2(F_o^2 + (0.0646P)^2 + 1.4543P]$ and $P = (|F_o|^2 + 2|F_c|^2)/3$, and the goodness of fit on F^2 was 1.063 for all observed reflections. For **4** convergence was reached at a final R1 = 0.0364 [for $I > 2\sigma(I)$], wR2 = 0.0956 [for all data], 315 parameters, with allowance for the thermal anisotropy for all non-hydrogen atoms. The weighting scheme employed was $w = [\sigma^2(F_o^2 + (0.0423P)^2 + 1.9317P]$ and $P = (|F_o|^2 + 2|F_c|^2)/3$, and the goodness of fit on F^2 was 1.030 for all observed reflections. Crystal data and details on the data collection and refinement are summarized in Table 1.

Spectral and Magnetic Measurements. IR spectra (4000−400 cm^{-1}) were recorded on KBr pellets with a Nicolet 250 FT-IR spectrometer. Magnetic measurements were carried out on polycrystalline samples with a Quantum Design MPMS SQUID susceptometer operating at a magnetic field of 0.1 T between 2 and 300 K. The diamagnetic corrections were evaluated from Pascal's constants.

Computational Method. In previous works, we have shown the ability of hybrid density functional methods to provide accurate numerical estimates of the exchange coupling constant J in transition-metal molecular complexes.[26−28] The B3LYP method is the most popular form of the so-called hybrid functionals,[29] in which the exact exchange, calculated using Kohn−Sham orbitals,[30] is mixed with the pure generalized gradient approximation (GGA)[31,32] functional. For this purpose we use the B3LYP method as implemented in the GAUSSIAN package[33] combined with a modified broken-symmetry approach. We have found that, when using DFT based wave functions, a reasonable estimate of the low spin state energy can be obtained directly from the energy of a broken-symmetry solution.[34] The J values are obtained using the following equation:

$$E_{HS} - E_{BS} = -(2S_1S_2 + S_2)J \quad (1)$$

where S_1 and S_2 are the total spins of the paramagnetic centers and $S_1 > S_2$ has been considered for heterodinuclear complexes. The reason of this procedure is the cancellation of the nondynamic correlation effects because they are introduced simultaneously by the commonly used functionals and also through the spin projections, as was explained recently by Polo et al.[35] A double-ζ basis set is used for the calculations including two p polarization functions for the copper and nickel atoms.[36] We have employed the experimental crystal structure, including hydrogen atoms, in order to keep the crystal packing effects.

Results and Discussion

Infrared Spectrum. At normal frequencies, the four complexes show the strong bands corresponding to the SCN$^-$ ligand (ν_a(CN) at 2100−2130 cm^{-1}), coordinate oxamidate group (ν_a(NCO) at 1610−1630 cm^{-1}), and ClO_4^- anion ($\nu_3(T_2)$ at 1120 cm^{-1} and $\nu_4(T_2)$ at 625 cm^{-1}) for complex **1** or PF_6^- anion ($\nu_3(T_{1u})$ at 865 cm^{-1} and $\nu_4(T_{1u})$ at 560 cm^{-1}) for complex **2**. Between 1600 and 400 cm^{-1} there are many bands attributable to the coordinated amine (tmen).

Description of the Structures. The structures of complexes **1** and **2** have the same cationic part but a different

(26) Ruiz, E.; Alemany, P.; Alvarez, S.; Cano, J. *J. Am. Chem. Soc.* **1997**, *119*, 1297.
(27) Ruiz, E.; Cano, J.; Alvarez, S.; Alemany, P. *J. Am. Chem. Soc.* **1998**, *120*, 11122.
(28) Cano, J.; Alemany, P.; Alvarez, S.; Ruiz, E.; Rodríguez-Fortea, A. *Chem. Eur. J.* **2000**, *6*, 327.
(29) Becke, A. D. *J. Chem. Phys.* **1993**, *98*, 5648.
(30) Parr, R. G.; Yang, W. *Density-Functional Theory of Atoms and Molecules*; Oxford University Press: New York, 1989.
(31) Becke, A. D. *Phys. Rev. A* **1988**, *38*, 3098.
(32) Lee, C.; Yang, W.; Parr, R. G. *Phys. Rev. B* **1988**, *37*, 785.
(33) Frisch, M. J., et al. *GAUSSIAN98*, rev. A.9; Gaussian, Inc.: Pittsburgh, PA, 1998.
(34) Ruiz, E.; Cano, J.; Alvarez, S.; Alemany, P. *J. Comput. Chem.* **1999**, *20*, 1391.
(35) Polo, V.; Kraka, E.; Cremer, D. *Theor. Chem. Acc.* **2002**, *107*, 291.
(36) Schaefer, A.; Horn, H.; Ahlrichs, R. *J. Chem. Phys.* **1992**, *97*, 2571.

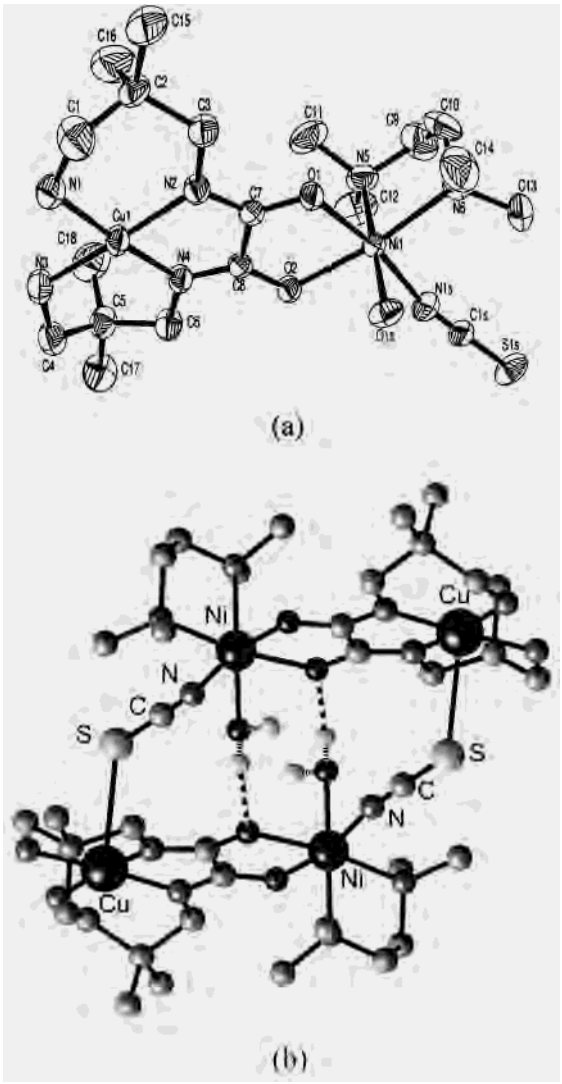

Figure 1. (a) ORTEP view of $[Cu(oxpn)Ni(\mu\text{-}NCS)(H_2O)(tmen)]_2(ClO_4)_2$ (**1**) with the atom-labeling scheme. Ellipsoids are shown at the 50% probability level. The complex $[Cu(oxpn)Ni(\mu\text{-}NCS)(H_2O)\ (tmen)]_2(PF_6)_2$ (**2**) shows a very similar structure. (b) Drawing of the common tetranuclear cationic part of **1** and **2**.

counteranion. An ORTEP view of complex **1** is shown in Figure 1a; the drawing for complex **2** is almost identical. Selected bonds lengths and angles for complexes **1** and **2** are listed in Tables 2 and 3, respectively. Their common cationic part consists of two dinuclear $[Cu(Me_2oxpn)Ni(H_2O)(tmen)]^{2+}$ entities linked in two ways. The first one is made by two SCN^- groups, and the second one is made by two hydrogen bonds between the hydrogen atoms of the coordinated water molecule (O1S) of the nickel(II) ion and the oxygen atom (O1) of the oxamidate bridge of the neighboring entity (Figure 1b). The atoms of the tetranuclear entities were related by an inversion center. The crystal structures consist of tetranuclear $[Cu(Me_2oxpn)Ni(\mu\text{-}NCS)(H_2O)(tmen)]_2^{2+}$ cations separated by perchlorate **1** or hexafluorophosphate **2** anions. The coordination polyhedron of Cu^{II} can be considered as a square pyramid with apical elongation (4 + 1) with a τ factor value of 0.047 for **1** and 0.014 for **2** ($\tau = 0$ for a square pyramid and $\tau = 1$ for trigonal bipyramid). The four nitrogen atoms of the Me_2oxpn organic

Table 2. Selected Bond Lengths and Angles (Å, deg) for Complex **1**

Cu(1)−N(1)	2.014(3)	Ni(1)−N(1S)	2.057(3)
Cu(1)−N(2)	1.958(3)	Ni(1)−O(1)	2.058(2)
Cu(1)−N(3)	2.019(3)	Ni(1)−O(2)	2.082(2)
Cu(1)−N(4)	1.971(3)	Ni(1)−O(1S)	2.152(3)
Ni(1)−N(5)	2.161(3)	N(1S)−C(1S)	1.153(5)
Ni(1)−N(6)	2.146(3)	C(1S)−S(1S)	1.646(4)
N(2)−Cu(1)−N(4)	83.41(12)	N(1S)−Ni(1)−O(1S)	88.08(12)
N(2)−Cu(1)−N(1)	93.73(13)	O(1)−Ni(1)−O(1S)	82.96(11)
N(4)−Cu(1)−N(1)	176.00(14)	O(2)−Ni(1)−O(1S)	90.42(11)
N(2)−Cu(1)−N(3)	173.14(15)	N(6)−Ni(1)−O(1S)	92.78(13)
N(4)−Cu(1)−N(3)	93.56(13)	N(1S)−Ni(1)−N(5)	95.66(14)
N(1)−Cu(1)−N(3)	88.98(14)	O(1)−Ni(1)−N(5)	93.53(12)
N(1S)−Ni(1)−O(1)	169.00(13)	O(2)−Ni(1)−N(5)	91.32(12)
N(1S)−Ni(1)−O(2)	92.69(12)	N(6)−Ni(1)−N(5)	84.95(14)
O(1)−Ni(1)−O(2)	81.05(9)	O(1S)−Ni(1)−N(5)	175.79(12)
N(1S)−Ni(1)−N(6)	95.66(13)	C(1S)−N(1S)−Ni(1)	168.6(3)
O(1)−Ni(1)−N(6)	91.15(12)	N(1S)−C(1S)−S(1S)	179.5(4)
O(2)−Ni(1)−N(6)	171.15(11)		

Table 3. Selected Bond Lengths and Angles (Å, deg) for Complex **2**

Cu(1)−N(1)	2.013(2)	Ni(1)−N(1S)	2.050(2)
Cu(1)−N(2)	1.953(2)	Ni(1)−O(1)	2.0514(18)
Cu(1)−N(3)	2.016(2)	Ni(1)−O(2)	2.0741(18)
Cu(1)−N(4)	1.963(2)	Ni(1)−O(1S)	2.142(2)
Ni(1)−N(5)	2.158(3)	S(1S)−C(1S)	1.643(3)
Ni(1)−N(6)	2.140(3)	N(1S)−C(1S)	1.145(4)
N(2)−Cu(1)−N(4)	83.65(9)	N(5)−Ni(1)−O(1S)	175.61(9)
N(4)−Cu(1)−N(3)	93.38(9)	O(2)−Ni(1)−O(1S)	90.84(8)
N(2)−Cu(1)−N(3)	174.52(10)	O(1)−Ni(1)−O(1S)	82.36(8)
N(4)−Cu(1)−N(1)	173.39(10)	N(6)−Ni(1)−O(1S)	93.12(10)
N(2)−Cu(1)−N(1)	93.67(9)	N(5)−Ni(1)−N(1S)	95.56(11)
N(3)−Cu(1)−N(1)	88.80(10)	O(2)−Ni(1)−N(1S)	92.79(9)
N(5)−Ni(1)−O(2)	90.80(9)	O(1)−Ni(1)−N(1S)	168.87(9)
N(5)−Ni(1)−O(1)	93.87(9)	N(6)−Ni(1)−N(1S)	96.30(10)
O(2)−Ni(1)−O(1)	81.17(7)	O(1S)−Ni(1)−N(1S)	88.43(9)
N(5)−Ni(1)−N(6)	84.63(11)	C(1S)−N(1S)−Ni(1)	171.5(3)
O(2)−Ni(1)−N(6)	170.18(9)	N(1S)−C(1S)−S(1S)	178.7(3)
O(1)−Ni(1)−N(6)	90.45(9)		

ligand are placed in the basal positions. The coordination is completed by the S atom of the SCN^- bridge at 3.004 Å for **1** and 3.013 Å for **2**. The Cu atoms are displaced from the least-squares basal plane toward the apical S atom by 0.033 Å for **1** and 0.075 Å for **2**. The Ni^{II} atoms are in a distorted octahedral environment. The two oxygen atoms of the Me_2-oxpn ligand, one nitrogen atom of the bidentate amine (tmen), and the nitrogen of the thiocyanate bridge occupy the four positions coplanar to the oxamidate bridge. The oxygen of the water ligand and one nitrogen atom of the bidentate amine occupy the two remaining positions. The angles formed by the Ni−S−Cu are 105.505° for **1** and 104.462° for **2**. The Cu−Ni distances through the oxamidate bridge are 5.333 Å for **1** and 5.311 Å for **2**, and those through the thiocyanate bridge are 6.335 Å for **1** and 6.292 Å for **2**.

The structures of complexes **3** and **4** consist of dimeric $[Cu(oxpn)Ni(\mu\text{-}NCS)(NCS)(tmen)]$ and $[Cu(Me_2oxpn)Ni(\mu\text{-}NCS)(NCS)(tmen)]$ units, respectively, linked via an SCN^- group giving a one-dimensional system. ORTEP views of complexes **3** and **4** are shown in Figure 2a,b, and the main bond lengths and angles are listed in Tables 4 and 5, respectively. For both complexes the Cu^{II} ions have a 4 + 1 environment, and the coordination polyhedron can be considered as a square pyramid with a τ factor value of 0.251 for **3** and 0.267 for **4**. The four nitrogen atoms of the

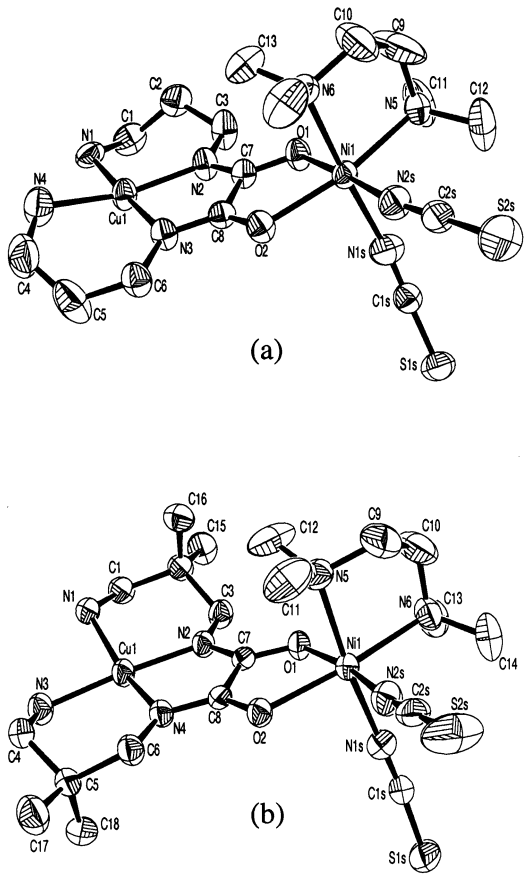

Figure 2. (a) ORTEP view of $[Cu(oxpn)(\mu\text{-}SCN)Ni(H_2O)(tmen)]_n$ (**3**) and (b) $[Cu(Me_2oxpn)(\mu\text{-}SCN)Ni(H_2O)(tmen)]_n$ (**4**) with the atom-labeling scheme. Ellipsoids are shown at the 50% probability level.

Table 4. Selected Bond Lengths and Angles (Å, deg) for Complex **3**

Cu(1)−N(1)	2.015(4)	Ni(1)−N(2S)	2.077(4)
Cu(1)−N(2)	1.970(4)	Ni(1)−O(1)	2.043(3)
Cu(1)−N(3)	1.953(3)	Ni(1)−O(2)	2.082(3)
Cu(1)−N(4)	2.022(4)	S(1S)−C(1S)	1.628(5)
Ni(1)−N(5)	2.160(3)	S(2S)−C(2S)	1.618(5)
Ni(1)−N(6)	2.190(4)	N(1S)−C(1S)	1.148(6)
Ni(1)−N(1S)	2.065(4)	N(2S)−C(2S)	1.157(6)
N(3)−Cu(1)−N(2)	83.56(14)	N(1S)−Ni(1)−N(5)	94.65(16)
N(3)−Cu(1)−N(1)	177.41(15)	N(2S)−Ni(1)−N(5)	92.54(14)
N(2)−Cu(1)−N(1)	93.85(15)	O(2)−Ni(1)−N(5)	168.80(12)
N(3)−Cu(1)−N(4)	91.96(16)	O(1)−Ni(1)−N(6)	92.22(13)
N(2)−Cu(1)−N(4)	162.35(18)	N(1S)−Ni(1)−N(6)	175.72(15)
N(1)−Cu(1)−N(4)	90.50(16)	N(2S)−Ni(1)−N(6)	89.39(15)
O(1)−Ni(1)−N(1S)	91.69(15)	O(2)−Ni(1)−N(6)	90.11(13)
O(1)−Ni(1)−N(2S)	176.94(14)	N(5)−Ni(1)−N(6)	83.61(14)
N(1S)−Ni(1)−N(2S)	86.78(16)	N(1S)−C(1S)−S(1S)	179.3(5)
O(1)−Ni(1)−O(2)	80.72(11)	N(2S)−C(2S)−S(2S)	178.5(5)
N(1S)−Ni(1)−O(2)	92.22(15)	C(1S)−N(1S)−Ni(1)	156.2(4)
N(2S)−Ni(1)−O(2)	96.68(13)	C(2S)−N(2S)−Ni(1)	164.3(4)
O(1)−Ni(1)−N(5)	90.23(12)		

oxamidate organic ligand are placed in basal positions, and the sulfur atom of the SCN^- group provides the pentacoordination. The Cu−S distance is 2.994 Å for **3** and 3.083 Å for **4**. The distance of the Cu^{II} atoms to the basal plane is 0.122 Å for **3** and 0.114 Å for **4**. For both complexes the Ni^{II} atoms are in a distorted octahedral environment. The four positions coplanar to the oxamidate bridge are occupied by the two oxygen atoms of this ligand, one nitrogen atom of the bidentate amine (tmen), and the nitrogen atom of the

Table 5. Selected Bond Lengths and Angles (Å, deg) for Complex **4**

Cu(1)−N(1)	2.023(2)	Ni(1)−N(2S)	2.053(2)
Cu(1)−N(2)	1.9479(19)	Ni(1)−O(1)	2.0653(15)
Cu(1)−N(3)	2.008(2)	Ni(1)−O(2)	2.1061(16)
Cu(1)−N(4)	1.9665(19)	S(1S)−C(1S)	1.635(3)
Ni(1)−N(5)	2.211(2)	S(2S)−C(2S)	1.629(3)
Ni(1)−N(6)	2.151(2)	N(1S)−C(1S)	1.147(3)
Ni(1)−N(1S)	2.080(2)	N(2S)−C(2S)	1.151(3)
N(2)−Cu(1)−N(4)	84.02(8)	O(1)−Ni(1)−N(6)	94.13(8)
N(2)−Cu(1)−N(3)	176.00(9)	N(1S)−Ni(1)−N(6)	91.00(9)
N(4)−Cu(1)−N(3)	94.03(8)	O(2)−Ni(1)−N(6)	173.51(8)
N(2)−Cu(1)−N(1)	92.48(8)	N(2S)−Ni(1)−N(5)	90.62(9)
N(4)−Cu(1)−N(1)	160.01(9)	O(1)−Ni(1)−N(5)	90.04(7)
N(3)−Cu(1)−N(1)	90.53(8)	N(1S)−Ni(1)−N(5)	174.26(9)
N(2S)−Ni(1)−O(1)	170.75(8)	O(2)−Ni(1)−N(5)	93.45(7)
N(2S)−Ni(1)−N(1S)	90.27(9)	N(6)−Ni(1)−N(5)	83.27(9)
O(1)−Ni(1)−N(1S)	90.00(8)	N(1S)−C(1S)−S(1S)	175.6(2)
N(2S)−Ni(1)−O(2)	90.52(8)	N(2S)−C(2S)−S(2S)	178.9(3)
O(1)−Ni(1)−O(2)	80.23(6)	C(1S)−N(1S)−Ni(1)	169.6(2)
N(1S)−Ni(1)−O(2)	92.22(8)	C(2S)−N(2S)−Ni(1)	174.3(2)
N(2S)−Ni(1)−N(6)	95.10(9)		

thiocyanate terminal ligand. The two remaining positions are occupied by the nitrogen atom of the thiocyanate bridge ligand and the other nitrogen atom of the bidentate amine (tmen). The dinuclear complexes are linked, in both complexes, through the *S*-thiocyanate ligand, which is directed toward the Cu^{II} atom of the neighboring dinuclear entity allowing a chain formation as shown in Figure 3a and Figure 3b for **3** and **4**, respectively. The Cu−Ni distance through the oxamidate bridge is 5.304 Å for **3** and 5.331 Å for **4**, and those through the thiocyanate bridge are 6.802 Å for **3** and 5.142 Å for **4**. The angles formed by the thiocyanate ligand and the Cu and Ni atoms are Ni(1)−N(1S)−C(1S) = 156.209°, Cu(1)−S(1S)−C(1S) = 119.836°, and Ni(1)−S(1S)−Cu(1) = 121.473° for **3** and Ni(1)−N(1S)−C(1S) = 169.609°, Cu(1)−S(1S)−C(1S) = 82.691°, and Ni(1)−S(1S)−Cu(1) = 77.530° for **4**; remarkable differences exist in the Ni−NCS−Cu angles in the two complexes. In complex **3**, three kinds of hydrogen bonds were found. There are intrachain hydrogen bonds between the nitrogen atom N(1) of the oxamidate ligand and the sulfur atom S(1S) of the thiocyanate ligand of the neighboring dinuclear entity through the H(1A) atom, the contact distance being N(1)···S(1S) = 3.201 Å (Figure 3a). Two sets of hydrogen interchains self-assemble themselves into two-dimensional supramolecular networks or layers (Figure 4). The S(1S) atom of the thiocyanate ligand and the N(4) atom of the oxamidate ligand are hydrogen-bond linked through H(4B), the contact distance being 3.589 Å; the N(2S) atom of the thiocyanate ligand and the N(1) atom of the oxamidate ligand are hydrogen-bond linked through H(1B), the contact distance being 3.252 Å. For complex **4**, only intrachain hydrogen bonds were found: one of them between the N(1) atom and the O(2) atom of the oxamidate ligand of the neighboring dinuclear through the H(1A), the contact distance being 3.258 Å, and the other between the N(3) atom and the O(2) atom of the oxamidate ligand of the neighboring dinuclear through the H(3A), the contact distance being 3.175 Å (Figure 3b).

Magnetic Studies. Variable temperature (2−300 K) magnetic susceptibility data were collected for microcrys-

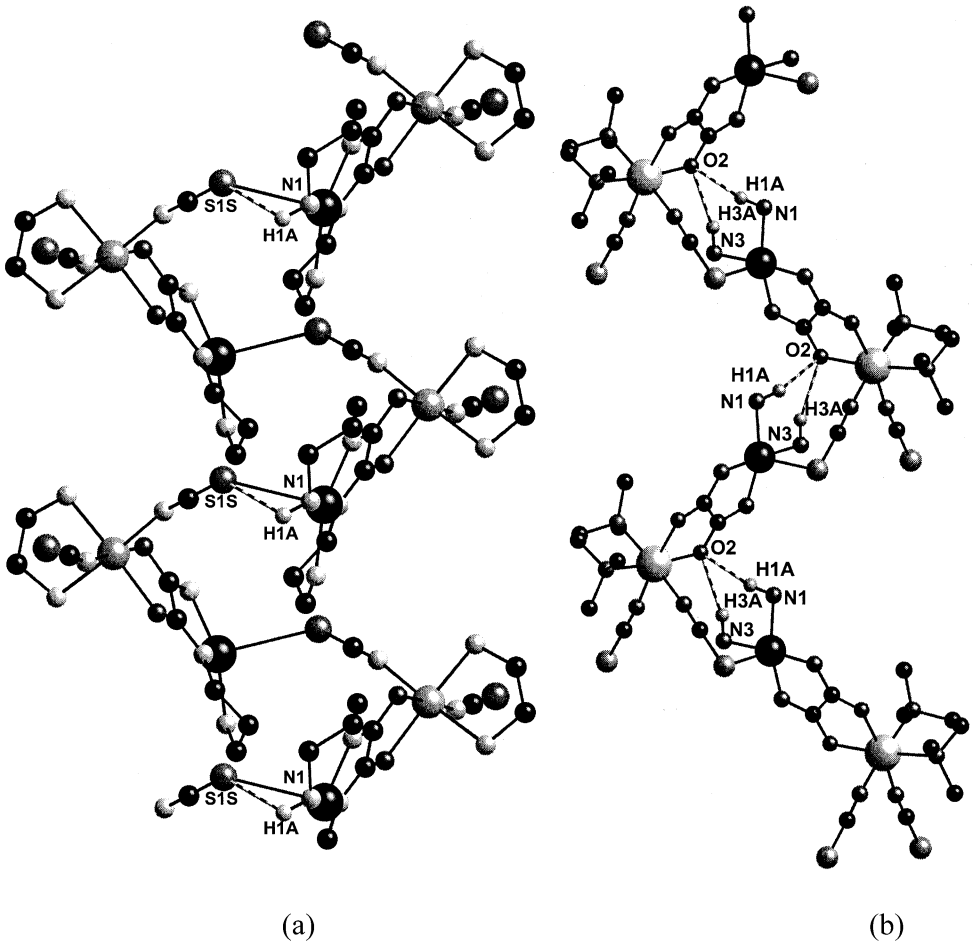

Figure 3. (a) Projection in the *xy* plane of the best view of the one-dimensional $[Cu(oxpn)(\mu\text{-}SCN)Ni(H_2O)(tmen)]_n$ (**3**) system and (b) projection in the *yz* plane of the best view of the one-dimensional $[Cu(Me_2oxpn)(\mu\text{-}SCN)Ni(H_2O)(tmen)]_n$ (**4**) system, showing, in both cases, the intramolecular-chain hydrogen bonds.

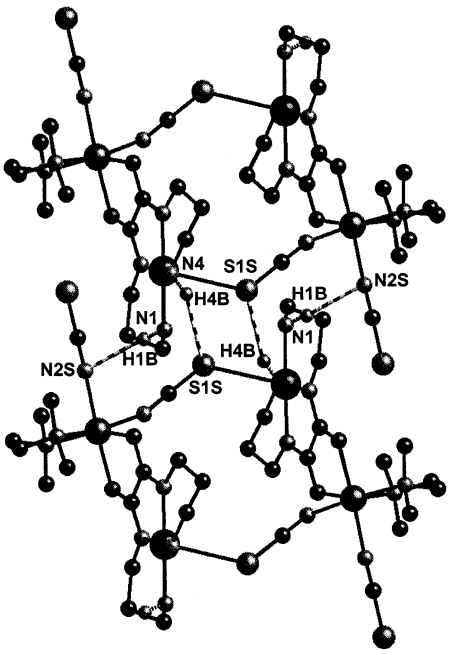

Figure 4. View of the self-assembly between two chains through hydrogen bonds in the *xz* plane of $[Cu(oxpn)(\mu\text{-}SCN)Ni(H_2O)(tmen)]_n$ (**3**).

talline samples of compounds **1**−**4** (Figures 5 and 6). From room temperature down to ca. 30 K for **1**, 45 K for **2**, and 25 K for **3** the $\chi_M T$ vs T plot corresponds to the classical behavior for an isolated Cu−Ni entity coupled antiferromagneticaly. Complex **4** shows a classic behavior for an isolated Cu−Ni entity coupled antiferromagneticaly in all temperature ranges (Figure 6b). A clear decrease in $\chi_M T$ appears from 30 K (0.45 $cm^3\ mol^{-1}\ K$) to 2 K (0.40 $cm^3\ mol^{-1}\ K$) for complex **1,** from 45 K (0.45 $cm^3\ mol^{-1}\ K$) to 2 K (0.35 $cm^3\ mol^{-1}\ K$) for complex **2**, and from 50 K (0.55 $cm^3\ mol^{-1}\ K$) to 2 K (0.44 $cm^3\ mol^{-1}\ K$) for complex **3**. The reduction of the $\chi_M T$ value in the low-temperature region for complexes **1**−**3** is indicative of intermolecular interaction through the SCN^- bridged ligand, or/and hydrogen bonds. Assuming a weak magnetic coupling between the dinuclear entities through the thiocyanate bridging ligand and/or the hydrogen bonds, the first fit was made to study exclusively the interaction between each Cu−Ni dinuclear complex in the range of temperature at which the behavior corresponded to isolated Cu−Ni dinuclear entities. The spin Hamiltonian that describes the isotropic magnetic exchange interaction in a Cu−Ni dinuclear complex is $H = -JS_{Cu}S_{Ni}$. There are two spin states, $S = {}^1/_2$ and $S = {}^3/_2$. Assuming antiferromagnetic coupling, the ground state is $S = {}^1/_2$ ($E = 0$) and the low-lying excited state is $S = {}^3/_2$ ($E = -3J/2$). The g values for each state are related to those of the ions: $g_{3/2} =$

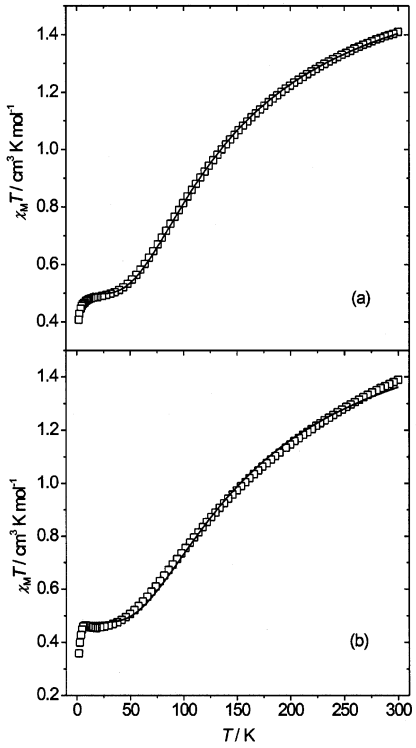

Figure 5. (a) Experimental and calculated variations of the $\chi_M T$ vs T for [Cu(oxpn)Ni(μ-NCS)(H_2O)(tmen)]$_2$(ClO_4)$_2$ (**1**). (b) Experimental and calculated variations of the $\chi_M T$ vs T for [Cu(oxpn)Ni(μ-NCS)(H_2O) (tmen)]$_2$-(PF_6)$_2$ (**2**).

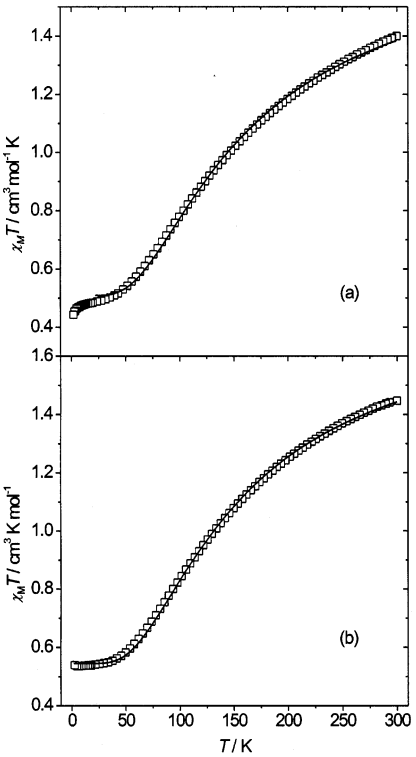

Figure 6. (a) Experimental and calculated variations of the $\chi_M T$ vs T for [Cu(oxpn)(μ-SCN)Ni(H_2O)(tmen)]$_n$ (**3**). (b) Experimental and calculated variations of the $\chi_M T$ vs T for [Cu(Me_2oxpn)(μ-SCN)Ni(H_2O)(tmen)]$_n$ (**4**).

$(1/3g_{Cu} + 2/3g_{Ni})$ and $g_{1/2} = (-1/3g_{Cu} + 4/3g_{Ni})$.[37] By introducing these values to the Van Vleck equation, a typical expression of the molar susceptibility can be deduced. The

Table 6. Best-Fit J and g Parameters for **1**−**4** from the Hamiltonian Given in the Text

compound	J (cm^{-1})	g_{Cu}	g_{Ni}	R^a
1	−107	2.20	2.27	2×10^{-5}
2	−119	2.28	2.26	2×10^{-4}
3	−116	2.19	2.29	9×10^{-5}
4	−113	2.16	2.35	4×10^{-5}

[a] $R = \sum_i(\chi_{M(calcd)}T - \chi_{M(obsd)}T)^2/\sum_i(\chi_{M(obsd)}T)^2$.

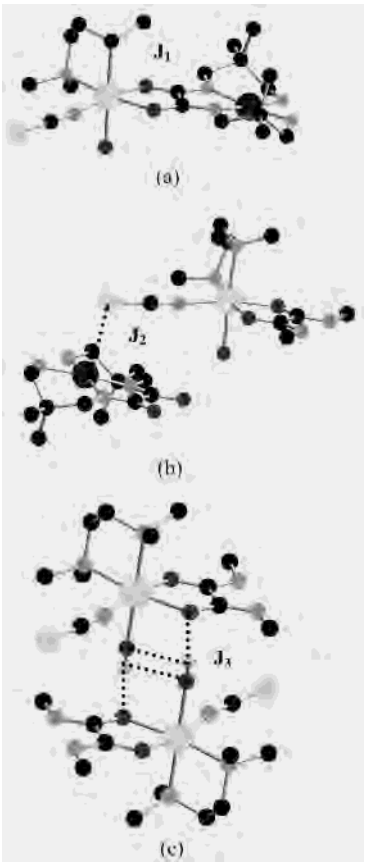

Figure 7. Structural models employed in the DFT calculations to study the three different exchange pathways: (a) that through the Me_2oxpn ligand, (b) that corresponding to the supramolecular interaction with the thiocyanate ligand, and (c) that between two Ni(II) cations through a double hydrogen bond.

experimental and theoretical curves of $\chi_M T$ versus T for complexes **1** and **2** are shown in Figure 5 and for complexes **3** and **4** are shown in Figure 6; the J and g values are listed in Table 6. The J values for the four complexes (close to -110 cm^{-1}) agree with those reported in the literature for Cu−Ni heterodinuclear complexes with the oxpn ligand.[21]

Theoretical Analysis of the Exchange Coupling. We focused our theoretical study on the exchange coupling interactions of complex [Cu(Me_2oxpn)Ni(μ-NCS)(H_2O)-(tmen)]$_2$(ClO_4)$_2$ (**1**). Due to the presence of different exchange pathways, we selected three different models from the crystal structure to analyze independently each coupling. In what that follows, we will call the models *a*, *b*, and *c*, respectively, to indicate those shown in Figure 7. The calculated exchange coupling constant for model *a* is $J_1 =$

(37) Bencini, A.; Gatteschi, D. *EPR of Exchange Coupled Systems*; Springer-Verlag: Berlin, 1990.

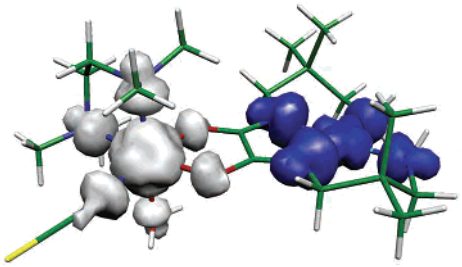

Figure 8. Spin density distribution for the Cu^{II} and Ni^{II} complex with an oxamidato bridging ligand (model *a*).

-121 cm^{-1}, which is in excellent agreement with the values reported for Cu−Ni heterodinuclear complexes with the oxpn ligand. The spin population map shows, due to the same sign in the spin population of the first coordination atoms, the predominance of the delocalization mechanism over the polarization mechanism (Figure 8). This is expected due to the antibonding nature of the metal orbitals bearing the unpaired electrons.

The other two interactions correspond to supramolecular pathways containing weak bond interactions such as the S···Cu contact in model *b* and a double hydrogen bond between the water molecules coordinated to the Ni(II) cations in model *c*. The calculated *J* values for models *b* and *c* are $J_2 = -0.14$ and $J_3 = -0.22$ cm^{-1}, respectively. Despite the fact that the magnitude of such couplings is beyond the limit of the accuracy of any theoretical method, it is interesting to point out that both couplings have a similar strength. Both supramolecular exchange pathways present small *J* values, but this is not a general rule. Thus, for instance, relatively strong exchange couplings are found in dinuclear Cu(II) complexes with exchange pathways containing hydrogen bonds.[38]

The analysis of the electronic structure shows, as expected, that the orbitals bearing the unpaired electrons are the $d_{x^2-y^2}$ in the Cu(II) cation and $d_{x^2-y^2}$ and d_{z^2} in the case of the Ni(II) center. These three orbitals corresponding to the quadruplet state of model *a* are shown in Figure 9. It is worth noting the high degree of localization of the orbitals due to the lack of symmetry of the complex and the presence of two different metal cations.

A clear magnitude that reveals the difference between the strengths of the exchange coupling of models *a* and *b* is the energy splitting of the three orbitals bearing unpaired electrons. Thus, for the quadruplet state of model *a* with the oxpn bridging ligand we found an energy splitting of 1.36 eV (which corresponds to the orbitals of Figure 9), but for model *b* with the SCN bridging ligand we found an energy splitting of only 0.25 eV. These values are in good agreement with the considerably stronger antiferromagnetic coupling of the oxpn bridging ligand assuming that the antiferromagnetic contribution depends on this energy splitting.[39]

The analysis of the structures of the polymeric complexes **3** and **4** shows that we have a similar exchange coupling for

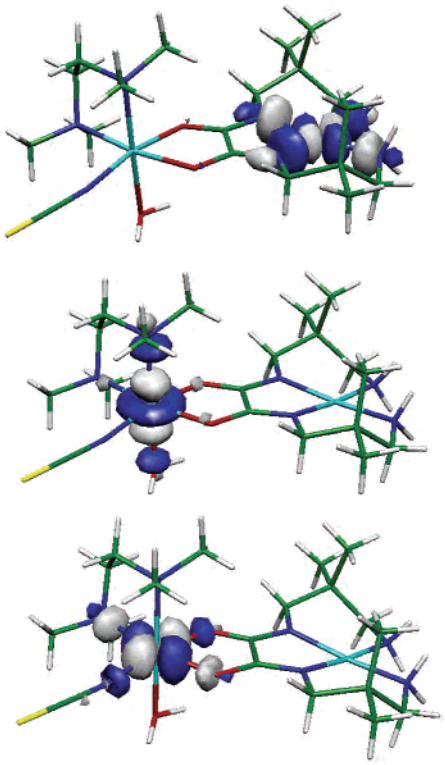

Figure 9. Molecular orbitals bearing the unpaired electrons of the model *a* (see Figure 7a) corresponding to the quadruplet state.

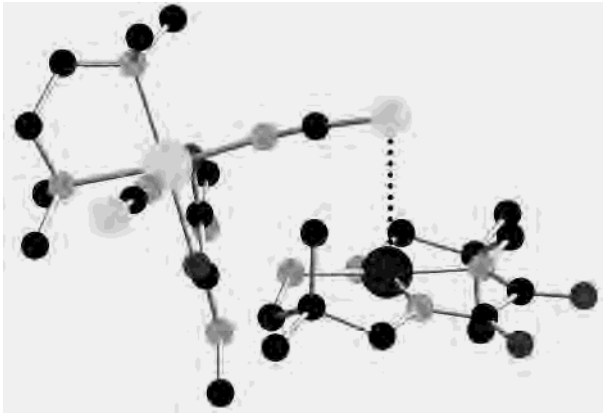

Figure 10. Structural model employed in the DFT calculations to study the exchange coupling through the thiocyanate bridging ligand in complex **4**.

the oxamidate bridging ligands. The structure of the exchange pathway through the thiocyanate ligand in the polymeric complex **4** is slightly different from in complex **1**. Thus, the C−S···Cu angle is 104.6° in complex **1** while it is only 82.7° in complex **4**, and the second main change is that the bridging thiocyanate ligand in complex **1** is coplanar with the oxpn ligand (equatorial coordination) but perpendicular to such ligands in complex **4** (axial coordination). In order to analyze such variations, we calculated the exchange coupling constant through the thiocyanate bridging ligand for complex **4** with the structural model shown in Figure 10. The calculated *J* value for this model is $+0.02$ cm^{-1}, which it is slightly smaller (absolute value) than that obtained for complex **1** with model *b* (-0.14 cm^{-1}). The smaller *J* value obtained for complex **4** agrees well with the experimental data, and

(38) Desplanches, C.; Ruiz, E.; Rodríguez-Fortea, A.; Alvarez, S. *J. Am. Chem. Soc.* **2002**, *124*, 5197.
(39) Hay, P. J.; Thibeault, J. C.; Hoffmann, R. *J. Am. Chem. Soc.* **1975**, *97*, 4884.

Scheme 1

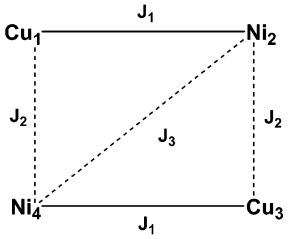

in order to clarify the difference between both structures, we calculated the J value for a modified model *b* of complex **1** taking the C−S···Cu angle of the complex **4**. The calculated J value for the modified *b* model is -0.20 cm^{-1}, which is similar to that obtained for the original model *b*. This result suggests that the variation in the exchange coupling through the thiocyanate bridging ligand between complexes **1** and **4** is probably due to the change of equatorial to axial coordination of such ligands with the Ni(II) cation instead of the different structure of the exchange pathway.

Correlations between Experimental and Theoretical DFT Calculations for 1. To compare the theoretical studies and the experimental magnetic behavior, simulations of the $\chi_M T$ vs T, using the CLUMAG program,[40] were performed. For the simulation, according to the structure of complex **1** given in Figure 1b, we assumed a ring of two copper(II) atoms and two nickel(II) atoms (Scheme 1). The J coupling parameters are defined as follows: J_1 corresponds to the coupling through the oxamidato bridge, J_2 to the coupling through the thiocyanate bridging ligand, and J_3 to the coupling through the hydrogen bonds (Figure 7). The simulations were performed according to the following Hamiltonian:

$$H = -J_1(S_1S_2 + S_3S_4) - J_2(S_2S_3 + S_1S_4) - J_3(S_2S_4) \quad (2)$$

In order to study the coupling through the thiocyanate ligand the simulation was performed by fixing the J_1 value as -110 cm^{-1}, $J_3 = 0$ and $g = 2.25$, and varying the values of J_2 between -1 and -10 cm^{-1} and between 1 and 10 cm^{-1}. The simulation is given in Figure 11a. It is important to note that when the J_2 value is antiferromagnetic, the $\chi_M T$ curve increases when the temperature is lowered, whereas it decreases when J_2 is ferromagnetic. In order to study the coupling through the hydrogen bonds, the simulation was performed fixing the J_1 value as -110 cm^{-1}, $J_2 = 0$ and $g = 2.25$, and varying the values of J_3 between -1 and -10 cm^{-1} and between 1 and 10 cm^{-1}. The simulation is given in Figure 11b. In this case, when the J_3 value is antiferromagnetic, the χ_MT curve decreases when the temperature is lowered, whereas it increases when J_2 is ferromagnetic. Thus, J_2 and J_3 exhibit opposite behavior. Finally, a simulation was made taking into account the theoretical values derived from the DFT studies: $J_1 = -121$ cm^{-1}, $J_2 = -0.14$ cm^{-1}, $J_3 = -0.22$ cm^{-1}, and $g = 2.26$. The resulting $\chi_M T$ vs T curve for dinuclear (Cu−Ni) unit, applying the theoretical values from the DFT calculation, is given in Figure 12, showing the qualitative agreement with the experimental data (Figure 12, inset).

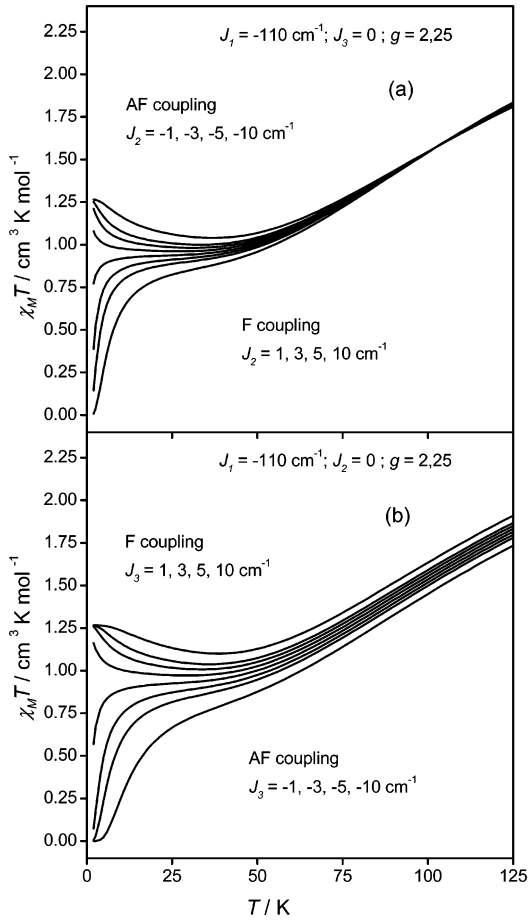

Figure 11. Theoretical curves obtained by CLUMAG program (see text): (a) for different values of J_2 considering $J_3 = 0$, (b) for different values of J_3 considering $J_2 = 0$. For both cases J_1 and g were constant: $J_1 = -110$ cm^{-1} and $g = 2.25$.

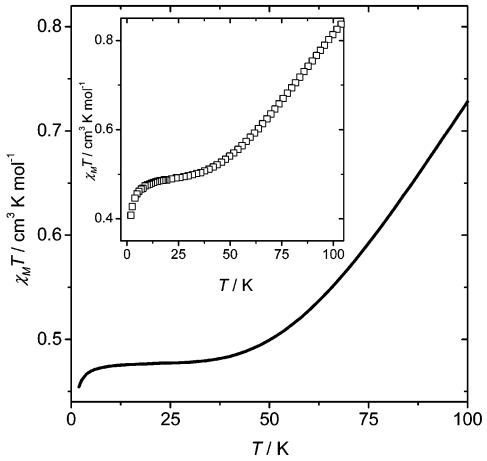

Figure 12. Theoretical curve obtained by CLUMAG program for the theoretical values from the DFT calculations: $J_1 = -121$ cm^{-1}, $J_2 = -0.14$ cm^{-1}, $J_3 = -0.22$ cm^{-1}, and $g = 2.26$. Inset: experimental data for [Cu(oxpn)Ni(μ-NCS)(H_2O)(tmen)]$_2$(ClO_4)$_2$ (**1**) (in the 100 K to 2 K range). In both cases the data are given for the dinuclear (Cu−Ni) unit.

(40) Gatteschi, D.; Pardi, L. *Gazz. Chim. Ital.* **1993**, *123*, 231.

Conclusions

(a) Structural Features. In this work we have synthesized four new complexes: $[Cu(Me_2oxpn)Ni(\mu\text{-}NCS)(H_2O)(tmen)]_2(ClO_4)_2$ (**1**), $[Cu(Me_2oxpn)Ni(\mu\text{-}NCS)(H_2O)(tmen)]_2(PF_6)_2$ (**2**), $[Cu(oxpn)Ni(\mu\text{-}NCS)(NCS)(tmen)]_n$ (**3**), and $[Cu(Me_2oxpn)Ni(\mu\text{-}NCS)(NCS)(tmen)]_n$ (**4**). By varying the stoichiometry of the thiocyanate anion, two kinds of complexes were obtained: tetranuclear and one-dimensional (considering only the SCN^- ligand). In the tetranuclear **1** and **2** complexes, the role of the counteranion is not important. In complexes **3** and **4**, the change of the oxamidato ligand (oxpn or Me_2oxpn) originates different self-assembled motives owing to hydrogen bonds.

(b) Magnetostructural Correlations. In the four cases, the coupling through the oxamidato ligand is the same, independent of the structure (tetranuclear, one-dimensional, or two-dimensional). For complex **1** (complex **2** is equivalent) the DFT calculations indicate that the coupling through the thiocyanate and hydrogen bonds is very small and antiferromagnetic. The low-temperature simulations of the $\chi_M T$ vs T give the opposite variation. The final simulation with the calculated values indicates that the coupling through the hydrogen bonds seems to be the dominating factor of the global coupling, resulting in a theoretical and experimental decrease in the $\chi_M T$ curve at low temperature. Complex **3** shows a decrease in the $\chi_M T$ curve at low temperature whereas complex **4** does not show this decrease. Theoretical studies with DFT for complex **4** give a negligible J value ($+0.02$ cm^{-1}) through the thiocyanate bridging ligand. This result suggests that the plateau in the $\chi_M T$ curve at low temperature could be explained either by negligible J values through the thiocyanate and hydrogen bonds or by very small J values but compensated owing to the opposite sense of their variation in the $\chi_M T$ vs T curve at low temperature (Figure 11). In complex **3**, the self-assembled structure through the thiocyanate ligand (axial coordination) is analogous to complex **4**. Taking into account, thus, that the J value is also negligible, the decrease in the $\chi_M T$ curve at low temperature will be due to the two-dimensional hydrogen bond's self-assembled structure, which is different and more complicated than in complex **4**.

Acknowledgment. This study was supported by Grant BQU2000/0791 from the Dirección General de Investigación Científica y Técnica (Spanish Government).

Supporting Information Available: Four X-ray crystallographic files, in CIF format. This material is available free of charge via the Internet at http://pubs.acs.org.

IC025910R